MID-AMERICA TRANSPORTATION CENTER

Report # MATC-MU: 278

Final Report

University of Nebraska Lincoln

K·STATE Kansas State University

KU THE UNIVERSITY OF KANSAS

MISSOURI S&T University of Science & Technology

LINCOLN University

University of Missouri

IOWA STATE UNIVERSITY

THE UNIVERSITY OF IOWA

Ground-based Interferometric Radar for Rockfall Hazard Monitoring

Brent L. Rosenblad, Ph.D., P.E.
Associate Professor
Department of Civil and Environmental Engineering
University of Missouri

Joseph Gilliam
Graduate Research Assistant

Francisco Gomez, Ph.D.
Associate Professor
Department of Geological Science

J.E. Loehr, Ph.D., P.E.
Associate Professor

Mizzou
University of Missouri

2015

MATC

Ground-based Interferometric Radar for Rockfall Hazard Monitoring

Brent L. Rosenblad, Ph.D., P.E.
Associate Professor
Department of Civil and Environmental Engineering
University of Missouri

Joseph Gilliam
Graduate Research Assistant
Department of Civil and Environmental Engineering
University of Missouri

Francisco Gomez, Ph.D.
Associate Professor
Department of Geological Sciences
University of Missouri

J.E. Loehr, Ph.D., P.E.
Associate Professor
Department of Civil and Environmental Engineering
University of Missouri

Technical Report Documentation Page

1. Report No. 25-1121-0003-278	2. Government Accession No.	3. Recipient's Catalog No.	
4. Title and Subtitle Ground-based Interferometric Radar for Rockfall Hazard Monitoring		5. Report Date May 6, 2015	
		6. Performing Organization Code	
7. Author(s) Brent L. Rosenblad, Joseph Gilliam, Francisco Gomez, J.Erik Loehr,		8. Performing Organization Report No. 25-1121-0003-278	
9. Performing Organization Name and Address Mid-America Transportation Center 2200 Vine St. PO Box 830851 Lincoln, NE 68583-0851		10. Work Unit No. (TRAIS)	
		11. Contract or Grant No.	
12. Sponsoring Agency Name and Address Research and Innovative Technology Administration 1200 New Jersey Ave., SE Washington, D.C. 20590		13. Type of Report and Period Covered 7/1/2013 to 12/31/2014	
		14. Sponsoring Agency Code MATC TRB RiP No. 34779	
15. Supplementary Notes			

16. Abstract

Rockfall events along transportation corridors are a major public safety hazard and can result in significant economic costs due to traffic delays and road repairs. Transportation agencies are in need of innovative technologies to identify and monitor rockfall hazards. Ground-based interferometric radar (GBIR) is an emerging remote-sensing technology that can be used to rapidly scan large regions and detect very small (millimeter-scale) surface deformations from small shifts in phase of the reflected radar signal. Previous applications of GBIR have focused primarily on monitoring large spatial movements, such as landslides, where the area of movement may be hundreds or thousands of square meters. Application of GBIR to rockfall hazards requires detecting minute movements occurring over a very small spatial scale (a few square meters). The objective of this study was to evaluate the threshold for detecting movements of individual boulders as a function of boulder size, the magnitude of movement, and the offset distance. Boulders, ranging from about 0.5 to 5 meters in surface dimensions, were moved in small mm-scale increments. Two GBIR devices setup at different viewpoints scanned a region covering approximately 20,000 m^2 after each controlled boulder movement. Interferograms developed from imagery collected before and after each movement of the largest boulders (2 m to 5 m in surface dimensions) showed clear phase anomalies associated with the boulder movement, while phase anomalies associated with movements of smaller boulders were not as clearly discernable. The movement magnitudes recorded with the GBIR were generally consistent with the expected values based on ground truth measurements.

17. Key Words Remote sensing, slope stability, rockfall		18. Distribution Statement	
19. Security Classif. (of this report) Unclassified	20. Security Classif. (of this page) Unclassified	21. No. of Pages 35	22. Price

Table of Contents

List of Figures

List of Tables

List of Abbreviations

Mid-America Transportation Center (MATC)
Nebraska Transportation Center (NTC)
Colorado Department of Transportation (CDOT)
Ground-Based Interferometric Radar (GBIR)

Acknowledgments

Disclaimer

The contents of this report reflect the views of the authors, who are responsible for the facts and the accuracy of the information presented herein. This document is disseminated under the sponsorship of the U.S. Department of Transportation's University Transportation Centers Program, in the interest of information exchange. The U.S. Government assumes no liability for the contents or use thereof.

Abstract

Rockfall events along transportation corridors are a major public safety hazard and can result in significant economic costs due to traffic delays and road repairs. Transportation agencies are in need of innovative technologies to identify and monitor rockfall hazards. Ground-based interferometric radar (GBIR) is an emerging remote-sensing technology that can be used to rapidly scan large regions and detect very small (millimeter-scale) surface deformations from small shifts in phase of the reflected radar signal. Previous applications of GBIR have focused primarily on monitoring large spatial movements, such as landslides, where the area of movement may be hundreds or thousands of square meters. Application of GBIR to rockfall hazards requires detecting minute movements occurring over a very small spatial scale (a few square meters). The objective of this study was to evaluate the threshold for detecting movements of individual boulders as a function of boulder size, the magnitude of movement, and the offset distance. Boulders ranging from about 0.5 to 5 meters in surface dimensions were moved in small mm-scale increments. Two GBIR devices setup at different viewpoints scanned a region covering approximately 20,000 m^2 after each controlled boulder movement. Interferograms developed from imagery collected before and after each movement of the largest boulders (2 m to 5 m in surface dimensions) showed clear phase anomalies associated with the boulder movement, while phase anomalies associated with movements of smaller boulders were not as clearly discernable. The movement magnitudes recorded with the GBIR were generally consistent with the expected values based on ground truth measurements.

Chapter 1 Introduction and Background

1.1 Overview of Interferometric Radar

Radar remote sensing is an active-source imaging technique. With a controlled source, radar images contain not only amplitude information from the reflected signal, but also phase information. If measurements are taken of the same scene at different times, the phase information in the radar images can be used to detect changes in the distance to the surface of the target of interest, as illustrated in figure 1.1. One cycle of phase shift (2π radians) corresponds with every half-wavelength of displacement in the line-of-sight (LOS) direction of the radar. Therefore the LOS deformation (δ) can be calculated from the phase difference (ϕ) and wavelength of the radar (λ) using:

$$\delta = \frac{-\lambda\phi}{4\pi} \tag{1.1}$$

The phase difference is determined by calculating the interferogram from two co-registered radar images of the same scene collected at different times.

Some of the most familiar applications involving interferometric analysis of data are from satellite-based Synthetic Aperture Radar (SAR), a technique generally referred to as "InSAR." InSAR has been primarily applied to large-scale earth movements, such as those associated with earthquakes (e.g., Massonnet et al., 1993), volcanoes (e.g., Massonnet et al., 1995; Pritchard and Simons, 2004) and ground subsidence from oil or groundwater withdrawal (e.g., Fielding et al., 1998; Schmidt and Burgmann, 2003). However, there are several shortcomings of satellite-based InSAR that limit its effectiveness for many civil engineering applications. First, interferometry is a "repeat-pass" technique that is subject to the repeat times of satellite orbits. The long repeat

times of satellite measurements (weeks to months) do not allow for the monitoring of deformations that occur over shorter time periods. Secondly, the data quality is often adversely affected by the large baselines (i.e. different locations) of the satellite measurements and significant atmospheric delay over the long travel path of the signal. These conditions add additional phase change terms that must be accounted for to detect the phase change due to surface movements. Third, the spatial resolution of the measurements is typically on the order of tens of meters, and is therefore not ideal for detecting small spatial settlement features associated with civil engineering infrastructure.
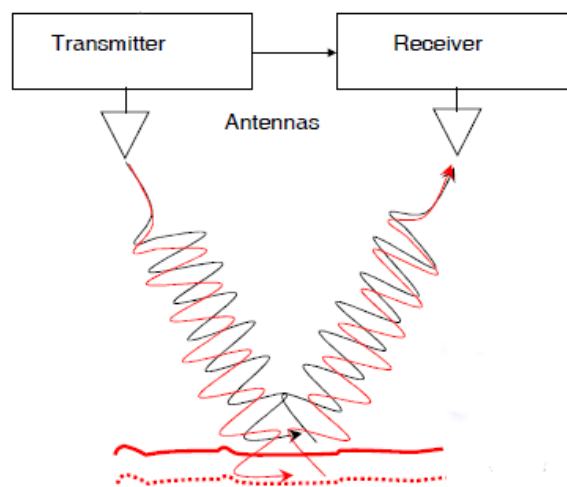
Figure 1.1 Schematic showing the relationship between surface movements and phase changes of the reflected radar signal

In recent years, ground-based interferometric radar (GBIR) systems have been developed and applied to measuring surface deformations. The operation of a GBIR is illustrated in figure 1.2. Ground-based interferometric radar operates in much the same way as satellite-based systems, but partially overcomes the three limitations listed above. First, it is possible to perform

repeat measurements on the order of minutes instead of months using GBIR. Second, GBIR has

a repeatable setup so baseline differences are negligible and atmospheric effects are significantly

diminished due to the shorter travel path. Last, because the device is located closer to the target,

the spatial resolution is significantly better than satellite-based measurements. GBIR is still an

emerging technology and is not in widespread use for civil engineering applications. Most of the

applications of GBIR have involved measuring deformations associated with large spatial-scale

movements, such as earth slopes and dams (e.g. Jenkins, 2013; Jenkins et al., 2012).
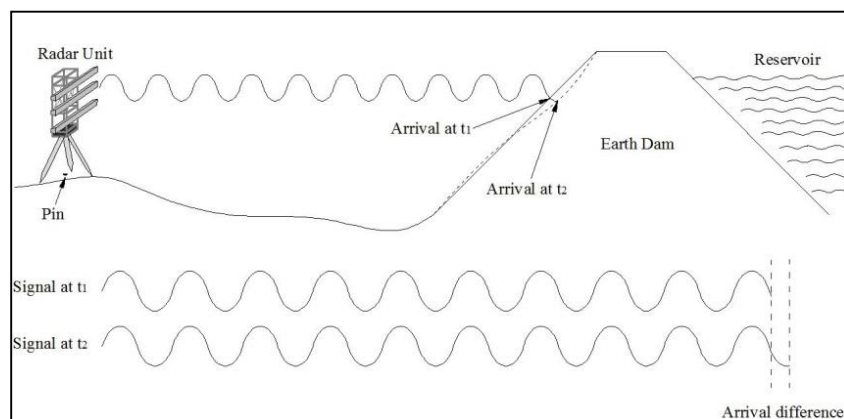
Figure 1.2 Schematic showing phase shift of reflected radar signal due to small movement of the

surface of an earth dam

1.2 GBIR System at the University of Missouri (MU)

       The GBIR system at MU is an enhanced version of the GPRI2 system built by Gamma

Remote Sensing. The GBIR consists of three antennae (two receiving and one transmitting)

mounted on a tower that is attached to a rotating platform, as shown in figure. 1.3. The entire

assembly is supported on a tripod. The radar is portable and can be removed and reset over the

same point. The MU GBIR has two frequencies (wavelengths) of operation: Ku-band

(wavelength 1.7 cm) and C-band (wavelength 5.6 cm). The measurements performed in this

study were made with the Ku-band radar, which is more sensitive to displacement and has better ground-pixel resolution. The GBIR operates by transmitting and receiving the radar signals while rotating at a rate of up to 10 degrees/sec. A 180-degree scan can be performed in less than 20 seconds. The GBIR can be operated at range offsets from 50 m to 7 km. At an offset of 100 m, the spatial resolution is approximately 0.75 m in both the range and azimuthal directions. The azimuthal resolution decreases at larger offsets.

Figure 1.3 GBIR system at the University of Missouri

1.3 Rockfall Overview

Rockfall is defined as loosened rock groups (blocks) or individual boulders initially present in vertical or steeply sloped faces of cuts, remote cliffs, or rock outcrops (Ladd, 1935). Cliffs of broken, faulted, or jointed bedrock on steep slopes of rocky soils are locations within the landscape where rockfall occurs (CGS, 2014). The severity of a rockfall event is categorized into four classifications: dribble of fine material, persistent fall of coarse material in the

formation of talus, falls of loosened rock from joints and faces, and occasional fall of massive single boulders or blocks (Ladd, 1935). The focus of this research is on the last category. Rockfall can be caused by a number of mechanisms or combination of mechanisms, including erosion, weathering, freeze-thaw cycles, and vegetation root-wedging.

Rockfall has been a persistent issue for populations living in mountainous landscapes with exposed rock slopes. Urban developments and transportation corridors in hazardous rockfall areas are a regular concern for geotechnical and geological engineers. Many regions of the Rocky Mountains in the U.S. are rockfall hazard areas. Throughout the Colorado Rocky Mountains the Colorado Geological Society (CGS) and Colorado Department of Transportation (CDOT) address rockfall hazards in urban areas and along transportation corridors. Since the 1980s, CGS and CDOT have responded to numerous rockfall events to remediate and mitigate damage to persons and property. Some locations impacted by these rockfall instances include Glenwood Springs, Booth Creek, Castle Rock, Manitou Springs, and I-70 in Glenwood Canyon (CGS, 2008). Direct costs in 2010 for the response to 14 rockfall and landslide incidents in Colorado were greater than $9,000,000 with indirect costs far exceeding this amount (USGS, 2010). Figure 1.4 illustrates the damage and boulder size perspective for a rockfall event in 2010 located along a transportation corridor in Colorado.

Figure 1.4 March 8, 2010 rockfall incident on I-70 in Glenwood Canyon Colorado

(USGS, 2010)

1.4 Motivation for this Study and Research Objectives

Studies documented in the existing literature conclude that GBIR is capable of accurately and effectively monitoring large-spatial scale slope movements. For example, GBIR has been shown to detect mm-scale deformations of a slow moving landslide in Colorado (Lowry et al., 2013). However, the potential application of GBIR for monitoring small, but localized movements within a massive landscape, such as the detection of movements of individual rock blocks and boulders, has not been studied. The primary objective of this research was to better understand the capabilities of GBIR for detecting small, localized movements within a massive landscape, specifically applied to rockfall hazard detection and monitoring. The specific objectives were to document the detectability threshold as a function of LOS movement, boulder size and offset distance. A secondary objective was to document the consistency between the magnitude of movements measured with the GBIR and those recorded using in-situ ground truth measurements.

6

Chapter 2 Measurement Site and Procedures

This chapter presents a description of the field test site, the experimental setup and data collection procedures, boulder descriptions, data processing methods, and displacement calculations. The controlled movement study was part of a study funded primarily by the Colorado Department of Transportation (CDOT) to evaluate rockfall monitoring capabilities of GBIR for use in detecting small, localized rock movements within a massive rock slope.

2.1 Site Description

The site for the controlled study is located approximately 30 miles west of Denver along a meander in Clear Creek (fig. 2.1). The area scanned by the GBIR systems was approximately 20,000 square meters of rock slope consisting of exposed rock faces and lightly vegetated areas. The control site was chosen because: (1) it allowed for the GBIR equipment to be set up at two vantage points, (2) it contained a wide variety of boulder sizes, and (3) the site was accessible for personnel to walk in the equipment used to move the boulders in a controlled manner. Twelve boulders, ranging in approximate facial dimensions from 0.5 to 5 meters, were selected for this study (fig. 2.2). These twelve boulders had range offset distances from 71 m to 152 m relative to the two GBIR locations. The general field of view of the scanned area from the GBIR 2 location (shown in fig. 2.2) is shown in figure 2.3.
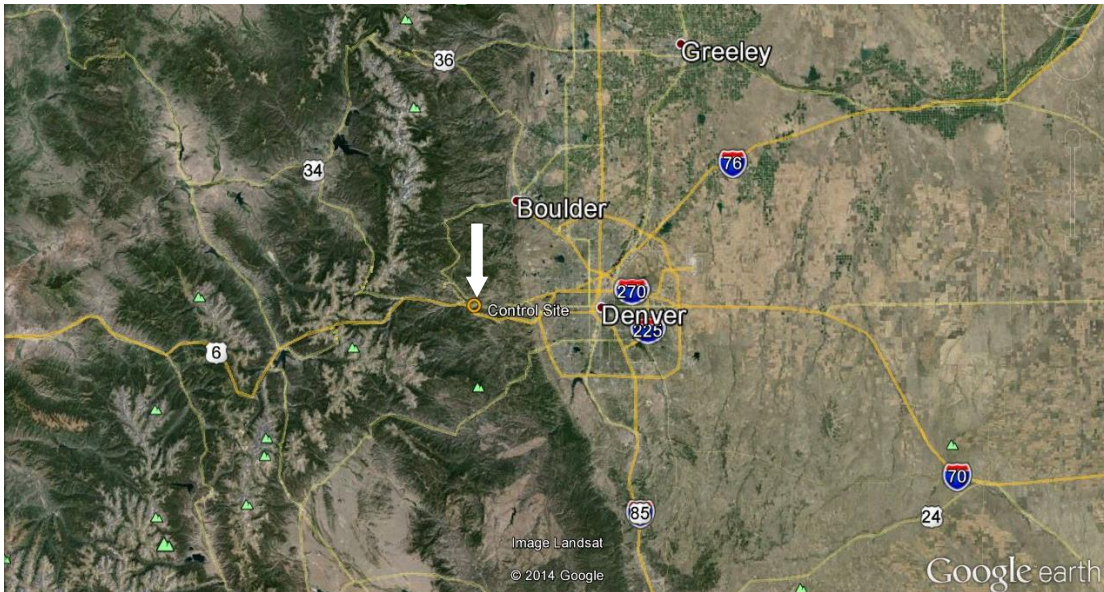
Figure 2.1 Google Earth image of control site location (white arrow)
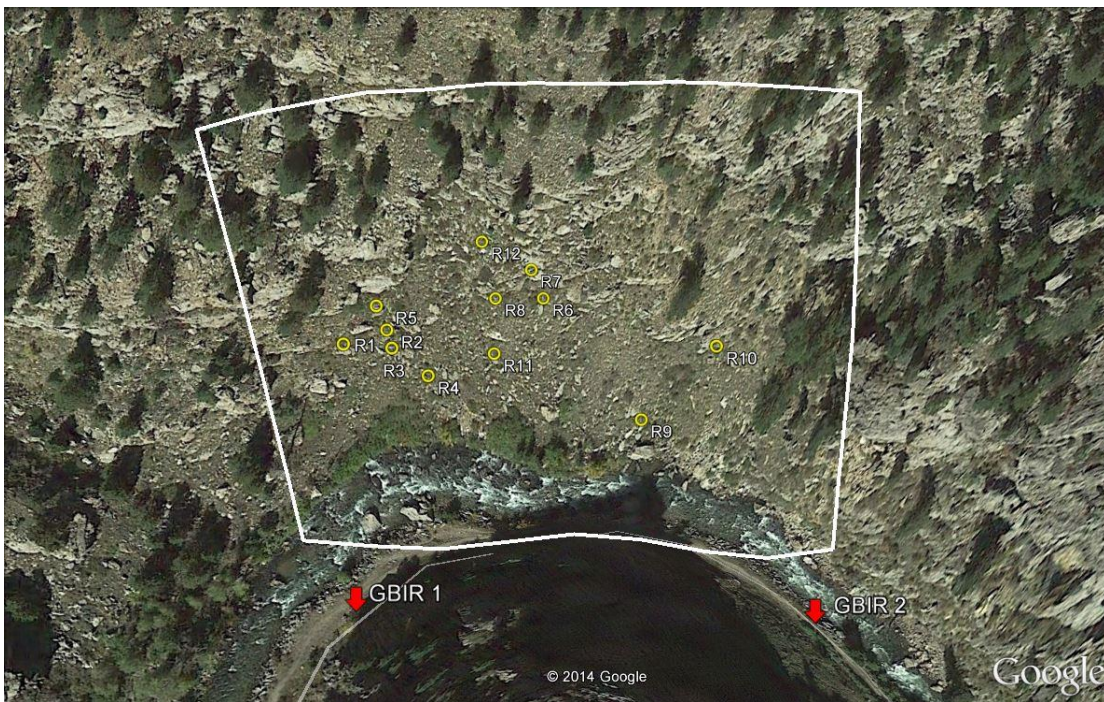
Figure 2.2 Google Earth image of control site showing the approximate scanned area (white outline), boulder locations (yellow circles) and the two GBIR set-up locations (red arrows)

Figure 2.3 View of the site from the GBIR 2 location

2.2 Experimental Setup and Data Collection Procedures

      Two GBIR systems were used in this study, one from MU and the other borrowed from the University of Arkansas. The GBIR systems were positioned at two locations on the point bar side of the meander. Standard setup and repeat setup procedures were used for consistent positioning of the GBIR systems over the respective survey pins at locations GBIR 1 and GBIR 2 (fig. 2.2). Both GBIR systems operated at scan rates of 5 degrees per second using Ku-band (17-mm wavelength) antennas fixed at 10 degree inclination angles.
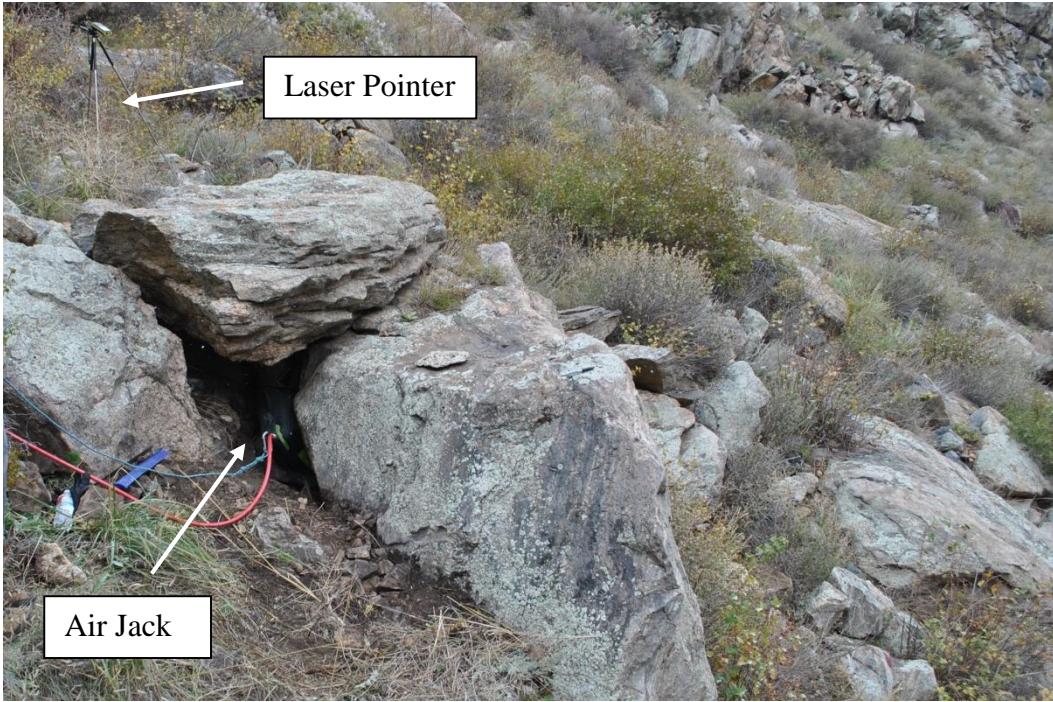
Figure 2.4 Typical setup scenario using the airbag jack and laser device

Figure 2.5 Typical movement path traced by laser (B – beginning; E - end)

Boulders were nudged in discrete increments using an airbag jack for large boulders and pry bars for smaller boulders. Small movement increments of a few mm were of particular interest, but movement increments up to 30 mm were also evaluated. After every increment of movement each GBIR system performed a scan set, which consisted of fours scans, and resulted in the collection of eight images (one from the top antennae and one from the bottom antennae for each of the four scans). This procedure was repeated for all boulders and movement increments. Before the first boulder was moved, a scan set was performed by each GBIR to provide a baseline image from each device. All subsequent images were resampled to the baseline images.

A total station was brought to the site to provide ground truth movement measurements. Unfortunately, the total station malfunctioned, so another approach was used to document the boulder movements. A stationary laser pointer device was positioned to shine a point on the respective boulders. After each push, the position on the boulder where the laser point was located was marked. A typical setup using the airbag jack and the laser device is shown in figure 2.4. Figure 2.5 shows a typical movement path traced by marking the laser point. After each increment of movement, in-situ ground truth measurements were taken by recording the length of the path traced on the boulder and the approximate direction of the movement using a handheld compass.

2.3 Boulder Descriptions

. Boulders were categorized into five size "bins" (<1m, 1-2m, 2-3m, 3-4m, 4-5m) according to the approximate surface dimensions of each boulder. Table 2.1 summarizes the approximate facial dimensions, the offset distance and azimuth direction for each boulder relative to the locations of GBIR 1 and GBIR 2.

Table 2.1 Boulder dimension and location information relative to GBIR locations

Boulder No.	Approximate Facial Dimensions (m)	GBIR 1		GBIR 2	
		Azimuth (º)	Offset (m)	Azimuth (º)	Offset (m)
1	<1	24.4	75.3	321.5	151.0
2	2-3	21.5	79.8	326	146.5
3	<1	24.8	74.7	322.7	140.0
4	<1	38.5	71.3	326.1	131.8
5	2-3	20.0	83.4	326.7	152.0
6	4-5	48.6	106.3	346.8	113.9
7	3-4	41.7	111.5	345.5	130.6
8	1-2	38.6	88.	338.1	132.0
9	1-2	64.7	99.7	347.3	82.9
10	<1	67.7	119.5	2.0	79.3
11	1-2	41.4	76.2	329.2	117.3
12	1-2	34.1	112.3	339.5	145.5.

2.4 Data Processing Methods

The GAMMA software package was used for data processing. The co-registration

commands in GAMMA were used to co-register all single look complex (SLC) files to the SLC

file from the first baseline scan taken. Coregistering all movement increment images to the first

image aligned all images into the same geometry. These coregistered SLCs are referred to as

resampled SLCs or RSLCs.

Interferograms were developed from the imagery (RSLC sets) collected before and after

various increments of movement. As noted above, a total of eight SLCs were collected in each

scan set performed following each increment of movement (four scans recorded on both the

upper and lower antennae). Eight raw interferogram images were created from the two RSLC

sets and were then averaged together using the "stacking" command to create a single stacked

raw interferogram. The stacked raw interferogram is an average of the eight raw interferograms with improved signal-to-noise values and phase estimations.

The boulder locations from each GBIR location were utilized to identify the pixels representing each boulder in the stacked interferograms. The boulder locations within the stacked interferograms were visually inspected to determine the boundary of pixels covering each boulder. Boulder pixels were identified by inspecting the stacked interferogram developed from each individual boulder movement increment. The phase values from the boulder pixels were recorded along with the phase values of the pixels surrounding the boulder pixels. Figure 2.6 demonstrates a general schematic of evaluated boulder pixels and surrounding pixels for each stacked interferogram. Recorded differential phase values range from $-\pi$ to π. Figure 2.7 provides a reference of differential phase value and its relationship to direction and magnitude of movement. A zero movement increment corresponds to zero radians of phase. For movement increments towards a GBIR location (positive) the phase values progress in a clockwise direction. For movement increments away from a GBIR location (negative) the phase values progress in a counterclockwise direction. The phase values "wrap" back to zero phase with every half-wavelength of movement.
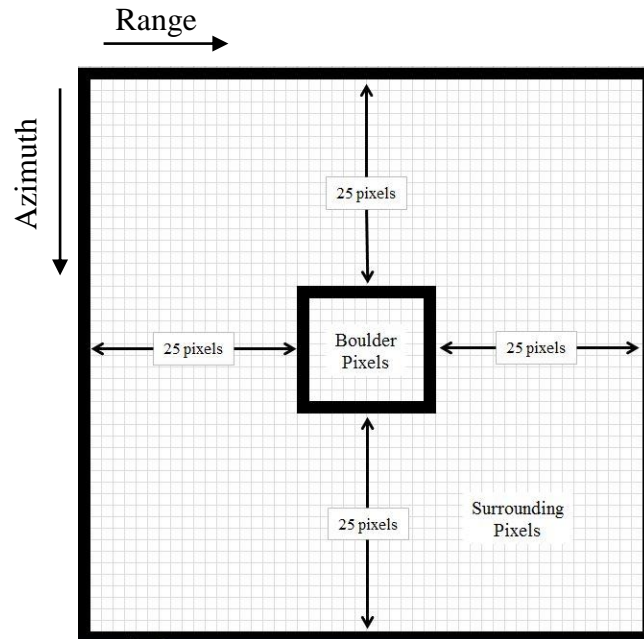
Figure 2.6 General schematic for boulder pixels and surrounding pixels selection using imagery in radar coordinates
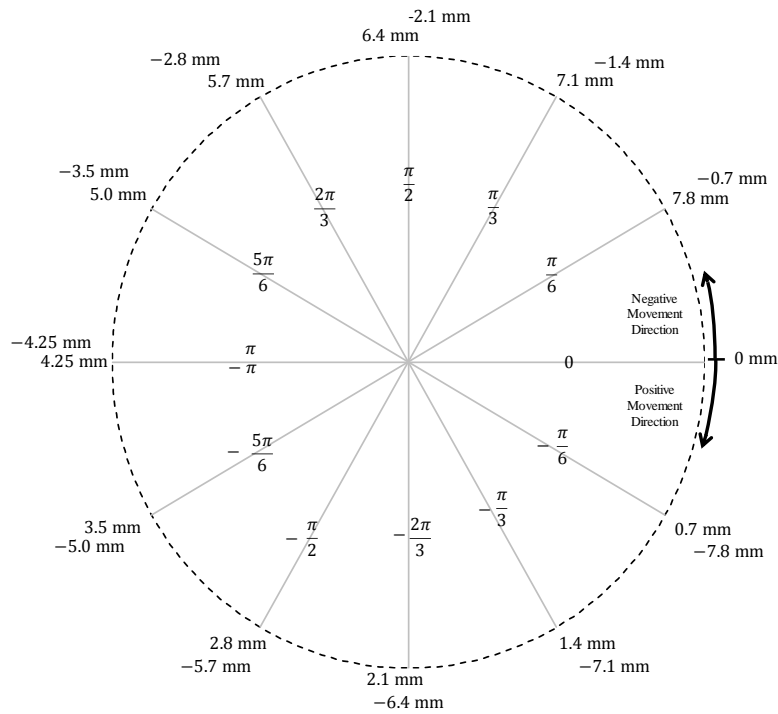

Figure 2.7 Relationship between measured phase, magnitude, and direction of movement

2.5 Determination of Detectability Threshold

       The primary objective of this study was to determine the threshold for detecting small movements of individual boulders using GBIR as a function of boulder size, magnitude of movements, and offset distance. Under ideal conditions, if no movement is occurring in the scene, all coherent pixels register a differential phase of zero (cyan color in the interferograms presented later). Therefore, the movement of an individual boulder covering only a few pixels should be apparent as a small region with non-zero phase values (unless the movement is exactly equal to one-half of the wavelength such that the phase value aliases to zero). In reality, the presence of vegetation and atmospheric effects produce other phase contributions in the scene. Therefore, a quantitative assessment of the detectability was performed by comparing the distribution of phase values over the region of movement to: (1) the distribution of phase values from surrounding pixels (see fig. 2.6), and (2) the distribution of phase values of the same pixels when the boulder was not moving. Boulder movements were considered detectable when a phase shift was observed in the phase distribution plots, as compared to the distribution of phase values from surrounding pixels and the distribution of phase values from the same boulder pixels when the boulder was not moved, as illustrated in the next section. Based on this criteria, the detectability was evaluated for several different increments of movement using a range of boulder sizes.

       A secondary objective was to compare the accuracy of the measurements to ground truth values. Due to the malfunctioning of the total station, the quality of the ground truth measurements was not sufficient to completely achieve this objective. However, comparisons were made between the measured phase values with the GBIR and those that would be expected

based on the estimated LOS movements obtained from the ground truth measurements. Sample

results from Boulder 7 and a summary of the findings are presented below.

Chapter 3 Results and Discussion

Twelve boulders were moved and monitored for this study. In this chapter the results

generated for one of the boulders (Boulder 7) are presented in detail and discussed to illustrate

the type of data and analyses that were used to assess the detectability of movements using

GBIR. The same procedures were followed and results generated for each of the twelve boulders

used in this study. A summary of the results obtained from all twelve boulders is presented and

discussed in this chapter. Detailed presentations of the results from each of the boulders can be

found in the thesis developed from this project (Gilliam, 2015).

3.1 Example Results– Boulder 7

Boulder 7 was located at an offset distance of 111 m from the locations of GBIR 1 and

131 m from the location of GBIR 2. Boulder 7 has surficial dimensions of approximately 4.3 m x

2.7 m x 0.9 m and has a near vertical crack, as shown in fig. 3.1. The air bag jack was inserted

into the crack and inflated to initiate outward movement of the boulder. Four increments of

movement were performed on this boulder. The first increment was 8 mm, the second and third

were 4 mm, and the forth increment was a backward movement of 4 mm due to the release of

pressure. Tables 3.1 and 3.2 summarize the different increments that were analyzed for Boulder

7. The notations B7-1, B7-2, B7-3, and B7-4 indicate the scan taken after each of the four

increments of movement. The notation B6-8 indicates the scan taken before Boulder 7 was

moved (i.e., the eighth and last increment of movement for Boulder 6). Interferograms were

generated from ten different combinations of scan pairs, as shown in tables 3.1 and 3.2. For

example, the notation B7-3_B6-8 indicates the interferogram developed between the scans taken

before Boulder 7 was moved (8th scan of boulder 6) and after the third increment of movement of

Boulder 7 (i.e. 16 mm of cumulative movement). The ground truth displacement in the line of

sight (LOS) of the radar (δ_{LOS}) was calculated from the measured ground truth displacement (δ_{GT}), the look direction of the radar to the boulder (θ_{RB}), and direction of boulder movement (θ_{GT}). For movement intervals where the LOS displacement was less than one-half wavelength the LOS displacement could be directly used to calculate the expected differential phase value ($\emptyset_E$). For cases where the expected LOS displacement was greater than one-half of the wavelength (one cycle of phase), the "normalized" LOS displacement was calculated by subtracting one-half of the wavelength (8.5 mm) from the LOS displacement. The actual phase measured by the GBIR ($\emptyset_M$) was used to calculate the measured LOS displacements (δ_{GBIR}).

The smallest of movement increments are of particular interest in this study. Therefore, example imagery is presented for the interferogram developed between scans B7-2_B7-1 recorded from GBIR 2, where the estimated LOS movement is 1.7 mm. Figure 3.2 shows a Google Earth image of the site with the interferogram superimposed on the image.

Figure 3.1 Photographs of Boulder 7 showing approximate width of the boulder (left) and near vertical crack behind the boulder where the air jack was inserted

Table 3.1 Boulder 7 In-Situ Ground Truth and GBIR 1 Measurements

Stacked Interferogram. ID	δ_{GT} (mm)	θ_{GT} (°)	θ_{RB} (°)	δ_{LOS} (mm)	Normalized δ_{LOS} (mm)	$\emptyset_E$ (rad)	$\emptyset_M$ (rad)	δ_{GBIR} (mm)
B7-1_B6-8	8	230	221.7	7.9	7.9	0.43	2.67	4.9
B7-2_B6-8	12	230	221.7	11.9	3.4	-2.49	0.35	8
B7-2_B7-1	4	230	221.7	4.0	4.0	-2.93	-2.36	3.2
B7-3_B6-8	16	230	221.7	15.8	7.3	0.86	-0.56	9.3
B7-3_B7-1	8	230	221.7	7.9	7.9	0.43	1.95	5.9
B7-3_B7-2	4	230	221.7	4.0	4.0	-2.93	-1.67	2.3
B7-4_B6-8	12	230	221.7	11.9	3.4	-2.49	1.01	7.1
B7-4_B7-1	4	230	221.7	4.0	4.0	-2.93	-1.79	2.4
B7-4_B7-2	0	230	221.7	0.0	0.0	0.00	0.57	-0.8
B7-4_B7-3	-4	230	221.7	-4.0	-4.0	2.93	2.31	-3.1

Table 3.2 Boulder 7 In-Situ Ground Truth and GBIR 2 Measurements

Stacked Interferogram. ID	δ_{GT} (mm)	θ_{GT} (°)	θ_{RB} (°)	δ_{LOS} (mm)	Normalized δ_{LOS} (mm)	$\emptyset_E$ (rad)	$\emptyset_M$ (rad)	δ_{GBIR} (mm)
B7-1_B6-8	8	230	165.5	3.4	3.4	-2.55	2.22	5.5
B7-2_B6-8	12	230	165.5	5.2	5.2	2.46	-0.26	8.9
B7-2_B7-1	4	230	165.5	1.7	1.7	-1.27	-2.21	3.0
B7-3_B6-8	16	230	165.5	6.9	6.9	1.19	-1.76	10.9
B7-3_B7-1	8	230	165.5	3.4	3.4	-2.55	2.63	4.9
B7-3_B7-2	4	230	165.5	1.7	1.7	-1.27	-1.37	1.9
B7-4_B6-8	12	230	165.5	5.2	5.2	2.46	0.61	7.7
B7-4_B7-1	4	230	165.5	1.7	1.7	-1.27	-1.50	2.0
B7-4_B7-2	0	230	165.5	0.0	0.0	0.00	0.70	-0.9
B7-4_B7-3	-4	230	165.5	-1.7	-1.7	1.27	2.06	-2.8

A close-in view of the interferogram is shown in fig. 3.3. A clear phase anomaly is apparent in the interferogram, which is consistent with the location of Boulder 7. Also, the magnitude of the phase is consistent with a movement of about 1.7 mm. Figure 3.4 shows the same interferogram presented in radar coordinates (range and azimuth) centered around Boulder

7 and surrounded by 25 pixels in each direction (see fig. 2.6). Interferograms from other scan set combinations are shown in figures 3.5 through 3.8.
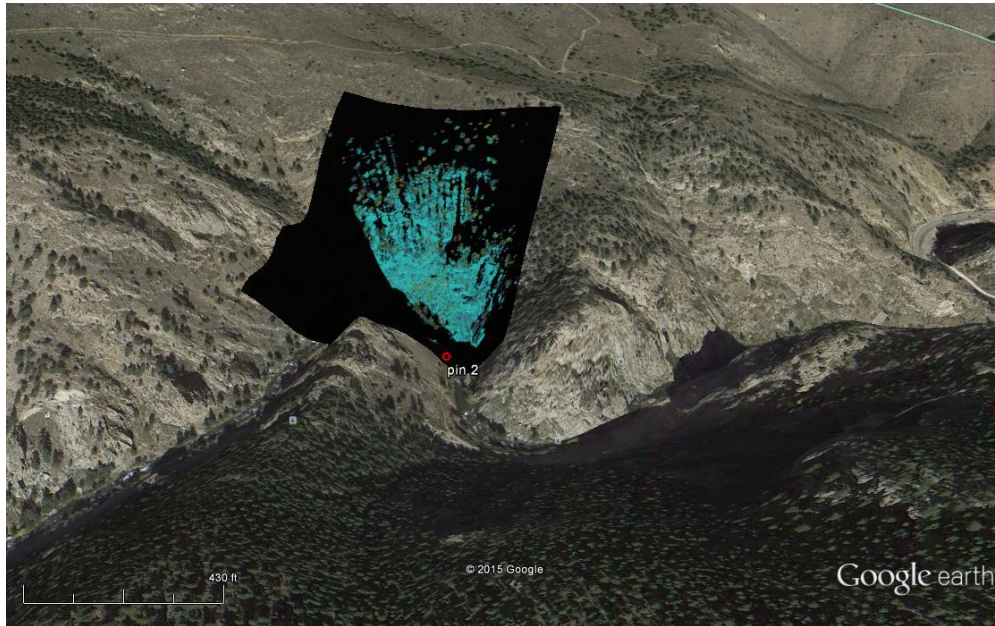

Figure 3.2 Google Earth image of field site with interferometric radar image superimposed
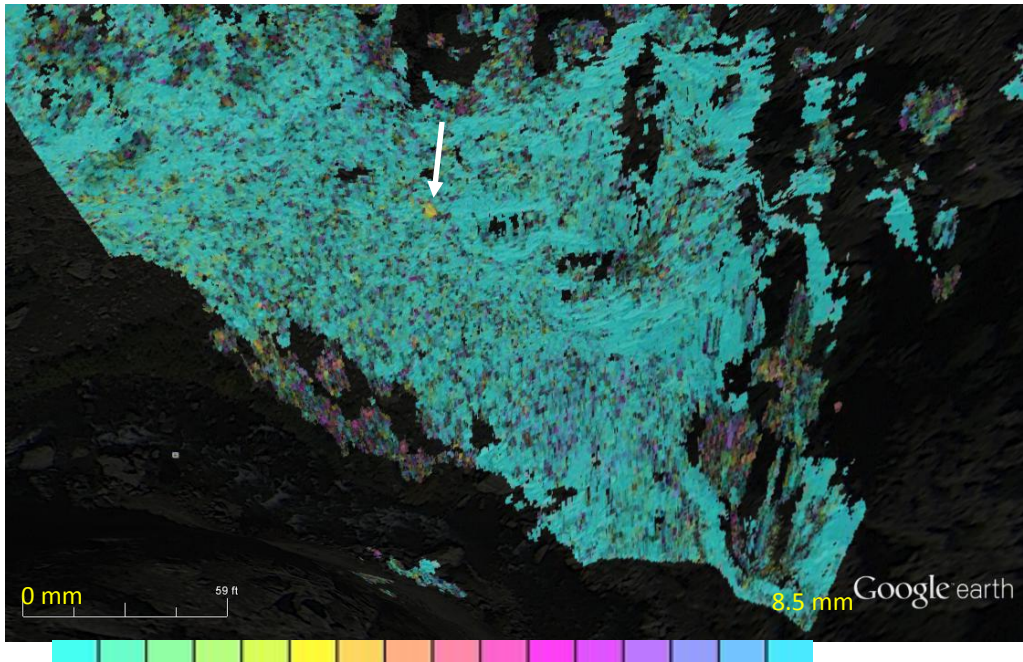
Figure 3.3 Close-in view of interferometric image in figure 3.2 showing the phase anomaly that

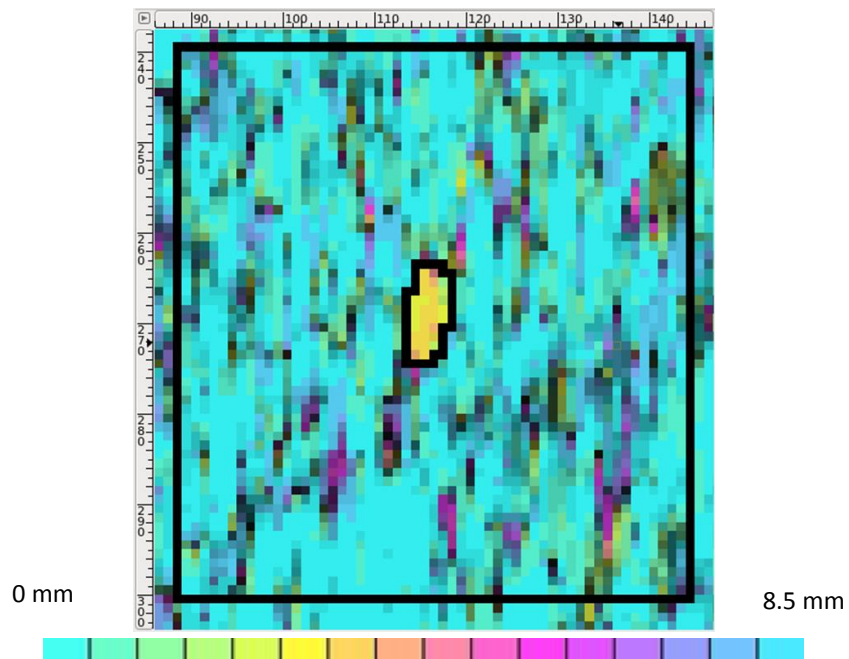is consistent with the location and magnitude of movement of Boulder 7

Figure 3.4 Close-in view of interferogram (in radar coordinates) centered around Boulder 7

developed from scan set 2 relative to scan set 1 (i.e., 1.7 mm of movement)

Figure 3.5 Close-in view of interferogram (in radar coordinates) centered around Boulder 7

developed from scan set 3 relative to scan set 1 (i.e., 3.4 mm of movement)

Figure 3.6 Close-in view of interferogram (in radar coordinates) centered around Boulder 7

developed from scans set 3 relative to scan set 2 (i.e., 1.7 mm of movement)

0 mm   8.5 mm

Figure 3.7 Close-in view of interferogram (in radar coordinates) centered around Boulder 7

developed from scans set 4 relative to scan set 2 (i.e., no net movement between scans)

-8.5 mm   0.0 mm

Figure 3.7 Close-in view of interferogram (in radar coordinates) centered around Boulder 7

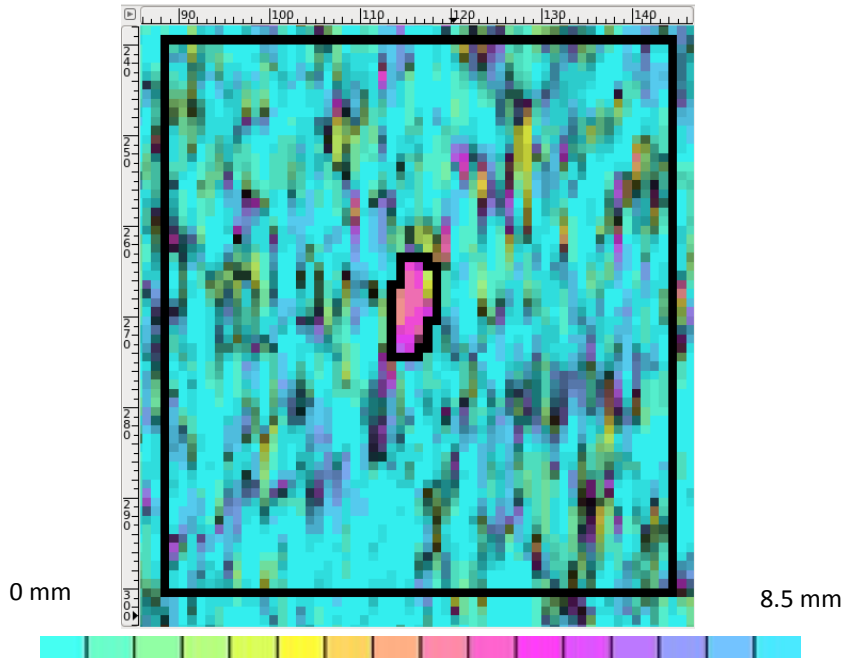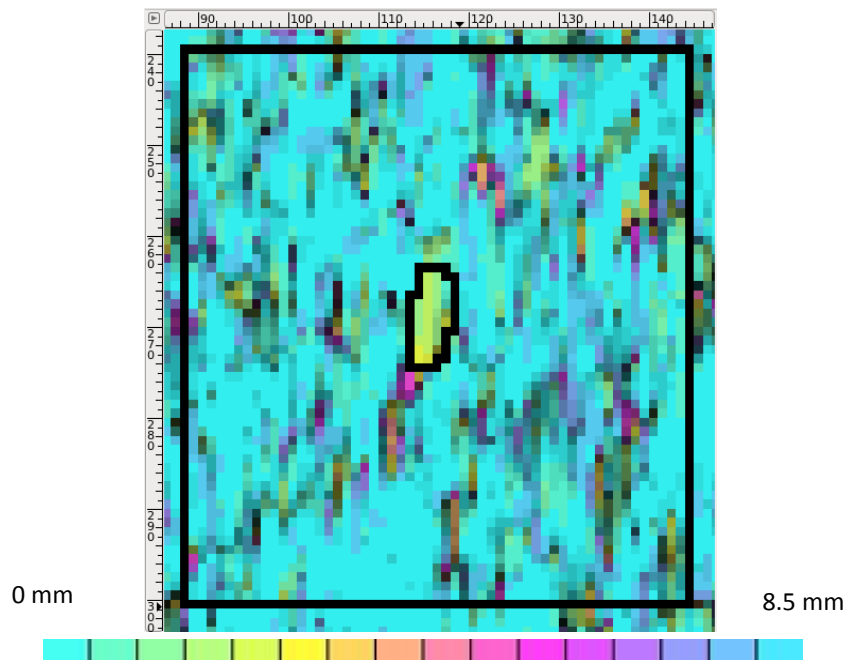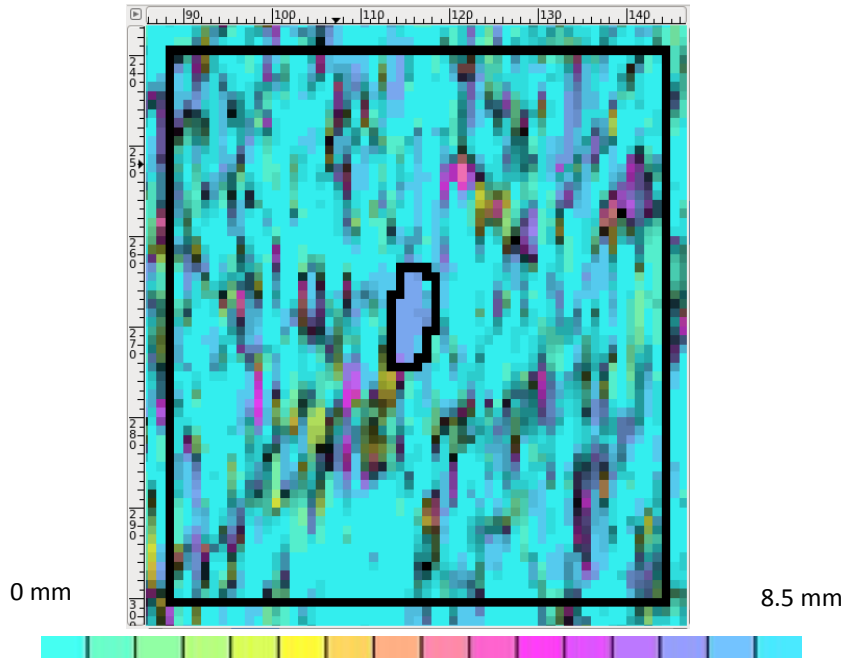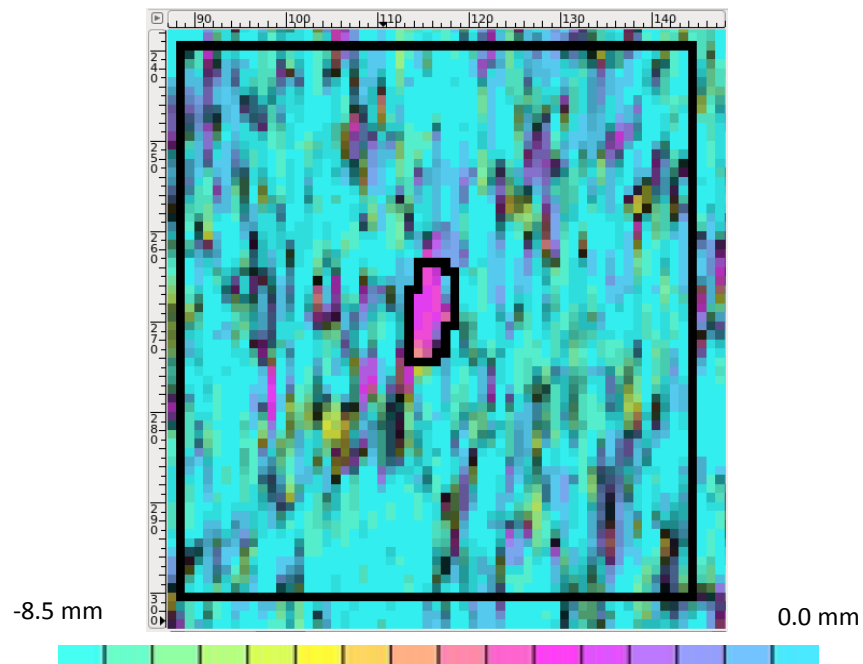developed from scans set 4 relative to scan set 3 (i.e., -1.7 mm of movement)

The results presented in figures 3.4 to 3.8 demonstrate that the GBIR can successfully track the small movements of Boulder 7. The phase anomalies change when the boulder is moved and the phase values are generally consistent with the expected values based on ground truth measurements. It should be noted that other phase anomalies are also present in these images. However, these anomalies are not persistent. These anomalies are likely due to the presence of vegetation on the slope. Future work will focus on developing methods to cull these portions from the image so that the phase anomaly of interest is clearly discernable.

To obtain a more quantitative assessment of the phase anomalies, cumulative distributions of phase values were compared between the boulder pixels and the surrounding pixels. This comparison is presented in figure 3.9. As expected, the surrounding pixels (dashed line) show a narrow distribution in phase values centered at a value of 0 (i.e., no movement), while the pixels on the boulder show non-zero values that are clearly differentiated from the non-moving surrounding pixels. Figure 3.10 presents a similar comparison between the boulder pixels and surrounding pixels when no movement was occurring (i.e. scans performed when other boulders were moved). As expected, the phase values were all centered around zero since no movement was occurring. Based on these results, it was determined that movements of Boulder 7 could be clearly detected using the GBIR 2 data. Similar analyses were performed for Boulder 7 from GBIR 1 and for each of the twelve boulders using interferograms measured from both locations. Detailed presentation of these results can be found in Gilliam, 2015. A summary of the findings from these studies is presented in section 3.2.

The measured phase values were also compared to the predicted phase values estimated from the ground truth measurements, as shown in figure 3.11. The measured phase values show the expected "sawtooth" pattern from the wrapping of the phase values. Considering the

uncertainty in the ground truth values, particularly the push direction, the measured and

predicted values are generally in good agreement.

Figure 3.8 Comparison of cumulative distributions of phase values from Boulder 7 pixels (solid

lines) and from the surrounding pixels (dashed lines) when Boulder 7 was moved

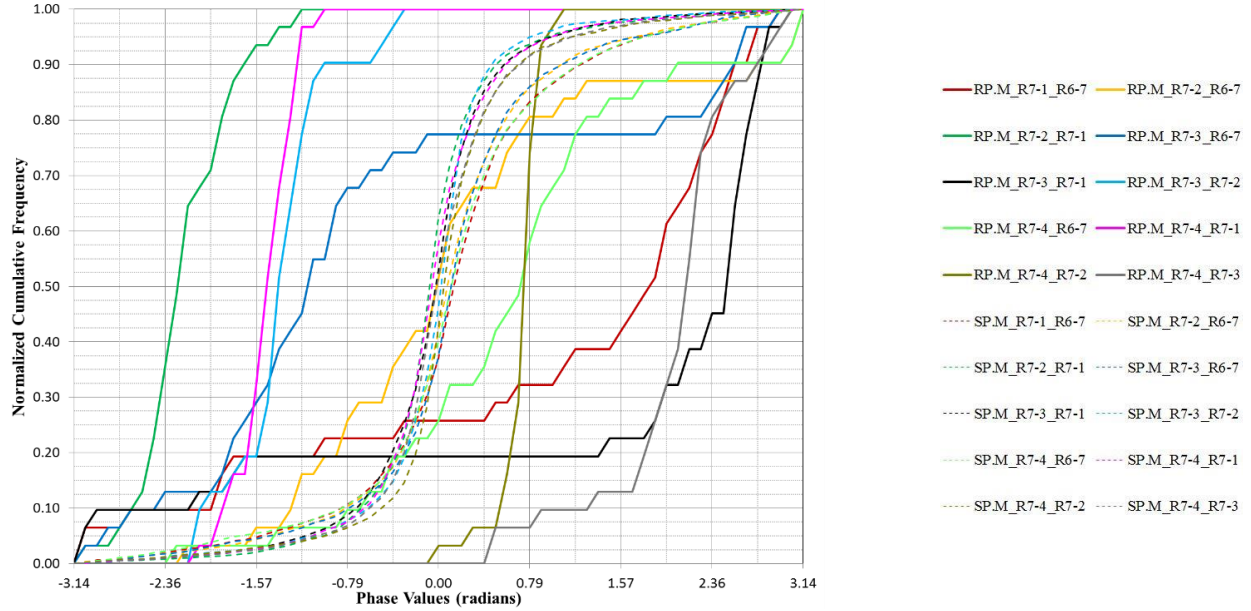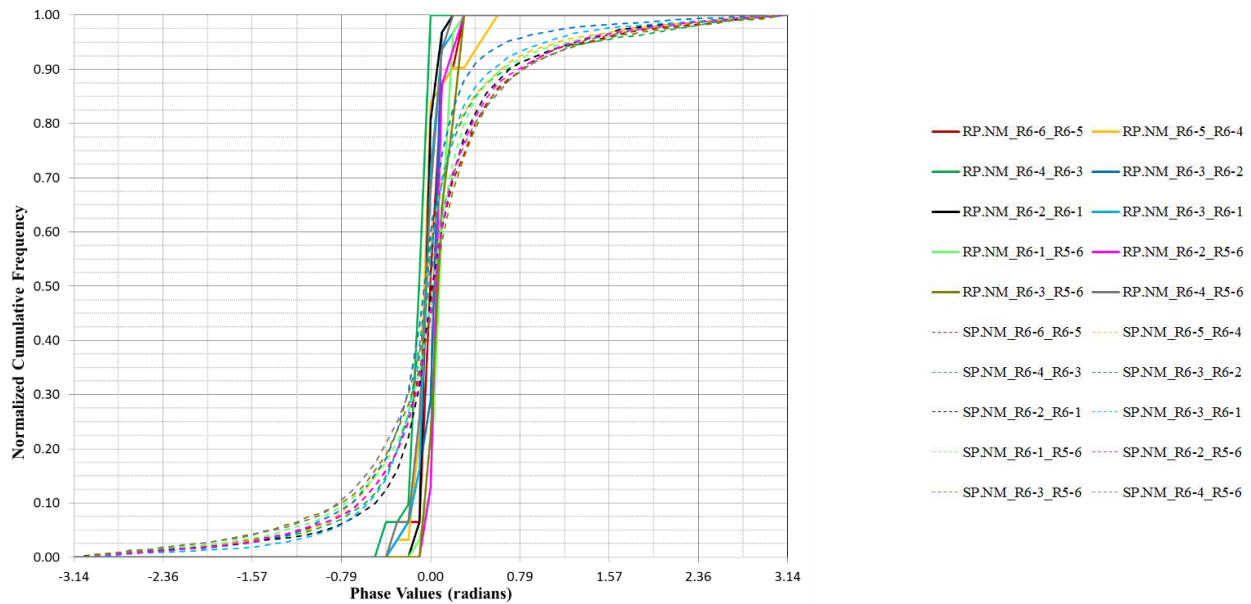**Figure 3.9** Comparison of cumulative distributions for phase values from Boulder 7 pixels (solid

lines) and from the surrounding pixels (dashed lines) when Boulder 7 was not moved
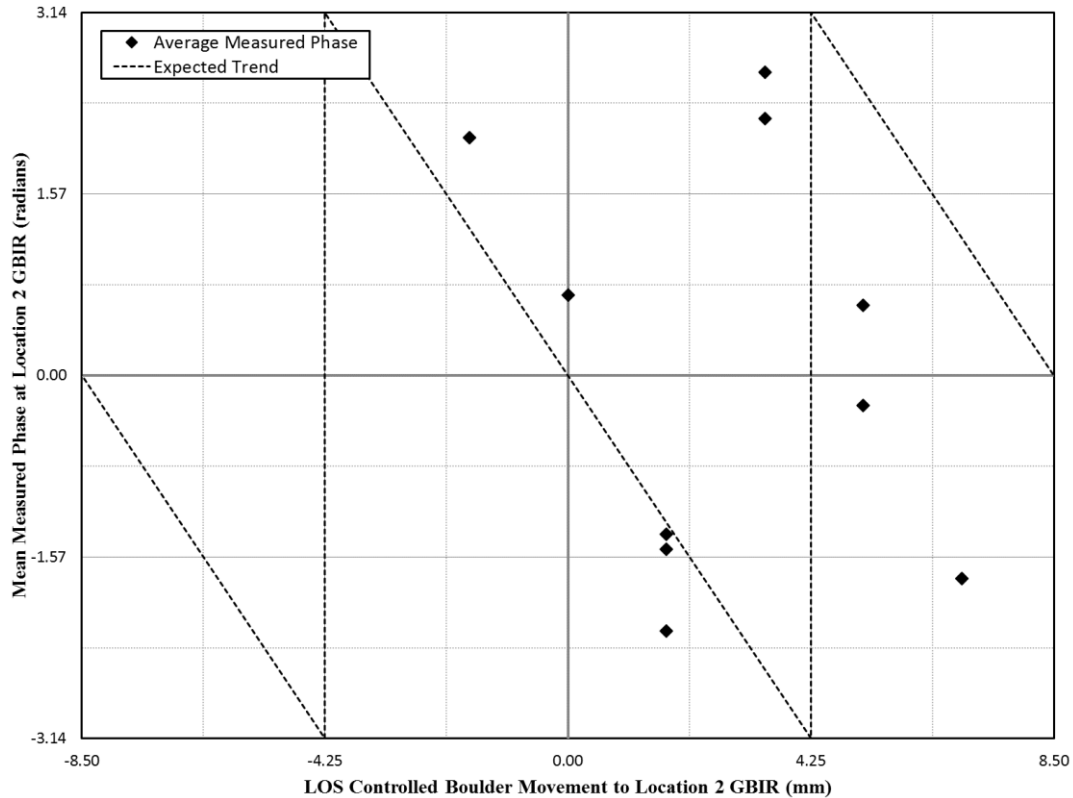
25

Figure 3.10 Comparison of predicted and measured wrapped phase values for movements performed on Boulder 7

3.2 Summary of Detectability Thresholds

The boulders used in this study were categorized based on their surface dimensions (see table 2.1). Each of the twelve boulders were placed into one of five boulder-size "bins" – 0-1m, 1-2m, 2-3m, 3-4m and 4-5m. The analyses described above for Boulder 7 were performed for each of the twelve boulders evaluated in this study and their detectability using GBIR was evaluated. Figure 3.12 presents a summary plot for measurements performed from GBIR 1 showing the detectability as a function of boulder size and magnitude of movement. Figure 3.13 presents the same data as a function of offset distance and magnitude of movement. The same plots are presented in figures 3.14 and 3.15, respectively, for measurements performed from

GBIR 2. Detectable movements are indicated with a solid symbol and movements that were not clearly detectable are indicated using an open symbol.

Figure 3.11 Detectability of movement as a function of boulder size and magnitude of movement (solid symbols – detectable; open symbols- not clearly detectable) for measurements recorded from GBIR 1

Figure 3.12 Detectability of movement as a function of magnitude of movement and offset

distance (solid symbols – detectable; open symbols- not clearly detectable) for measurements
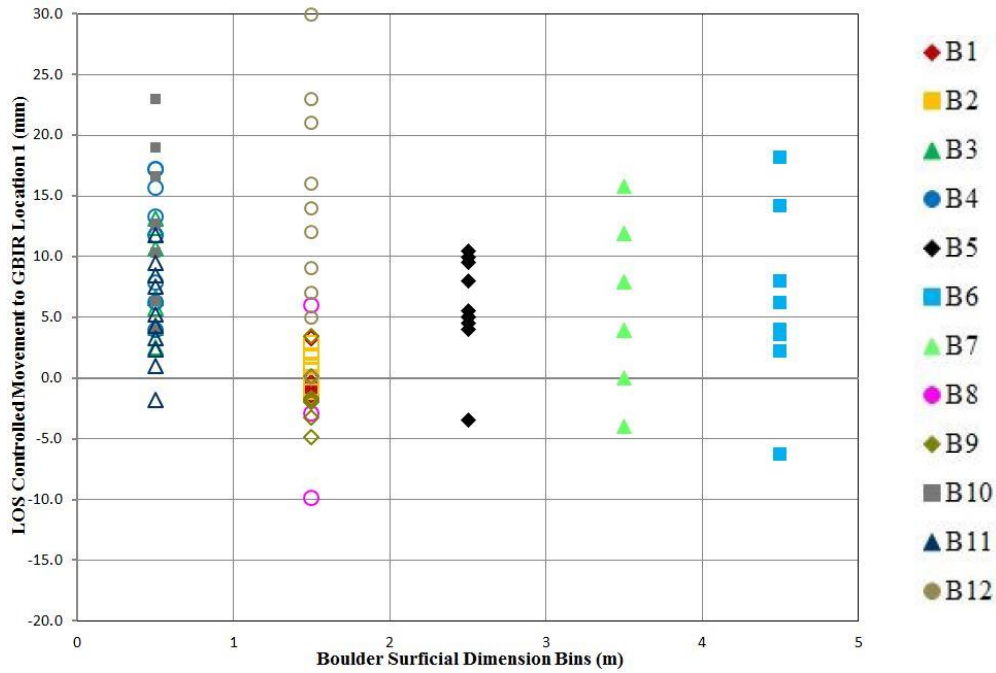
from GBIR 1

Figure 3.13 Detectability of movement as a function of boulder size and magnitude of movement (solid symbols – detectable; open symbols- not clearly detectable) for measurements from GBIR 2
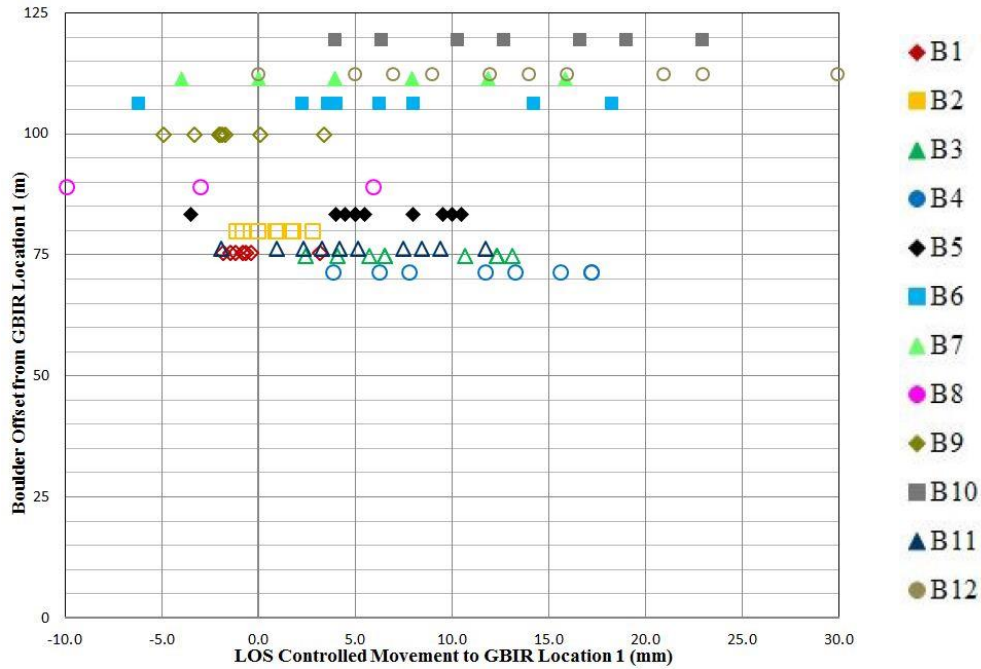
Figure 3.14 Detectability of movement as a function of magnitude of movement and offset distance (solid symbols – detectable; open symbols- not clearly detectable) for measurements from GBIR 2
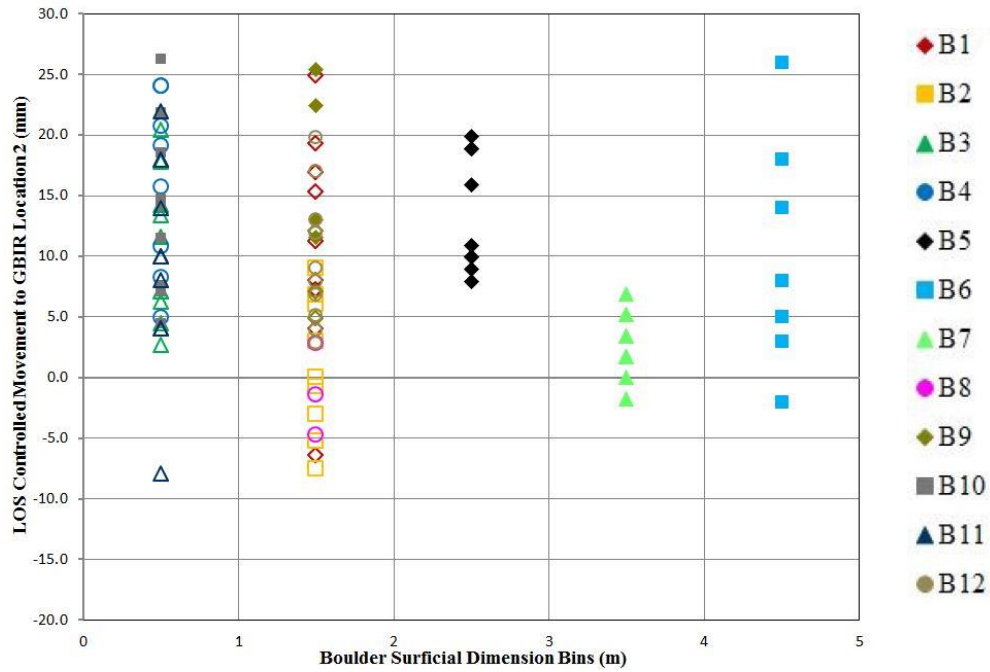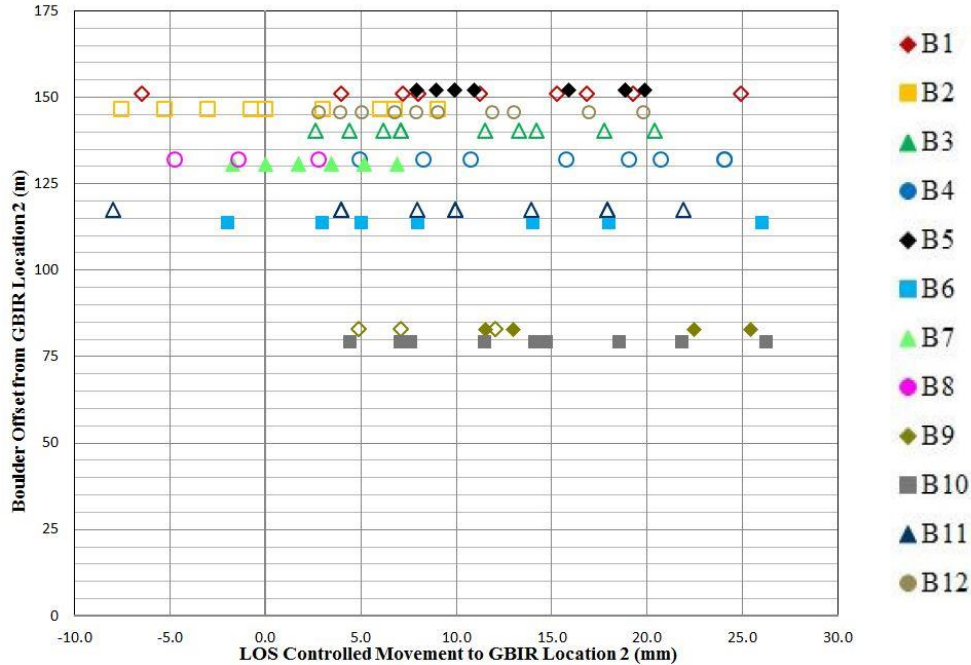
The results show that the detection of movement was primarily affected by the size of the boulder. Movements of the three boulders with dimensions of approximately 2 m or larger were detected for every increment of movement. The detectability was not a function of the magnitude of movement, as results from both GBIR 1 and GBIR 2 showed the smallest movements were detected as well as the largest movements. Movements as small as 1.7 mm were detected. This magnitude of movement is below the threshold of other remote sensing methods such as LiDAR and photogrammetry and therefore fills an important void in remote sensing measurements capabilities.

For boulders smaller than 2 m (i.e., those in the first and second bins), the results were mixed. Two of the nine boulders (B10 and B2) were deemed detectable using GBIR 1, and two

of the nine (B10 and B9) were deemed detectable using GBIR 2. For the other cases, the phase distributions from the moving boulder could not be clearly differentiated from either: (1) the phase distribution of pixels in the surrounding non-moving portion of the image, and/or (2) the distribution of the boulder pixels phase values when the boulder was not moved. The decrease in detectability performance as the size of the target decreased is not unexpected. The presence of vegetation around boulders produces phase anomalies that make it difficult to isolate and detect phase anomalies due to the boulder movement. This is especially true when the boulder is only covered by one or two resolution pixels, as was the case with the smallest boulders used in this study. Current work is being performed to improve the data collection and processing procedures to mitigate phase contributions from other sources.

It should also be noted that the findings from this study regarding detectable boulder sizes are only strictly applicable to the range offset distance used in this study (about 75 to 150 m). However, the results can be used to extrapolate the expected performance at larger range offset distances.

.

Chapter 4 Summary and Conclusions

4.1 Project Summary

      A controlled study was performed to assess the thresholds for detecting small boulder movements using GBIR. The study was performed on a rock slope located in a meander of Clear Creek in Colorado. Two GBIR radar systems were set up to scan the approximately 20,000 m^2 area of interest from two different vantage points. Twelve boulders ranging in dimensions from less than 1 m to over 5 m were selected to be used in this study. The boulders were moved in mm-scale increments using a pry bar for the smaller boulders and an air jack for the largest boulders. After each increment of movement the entire region was scanned from the two GBIR locations. Interferograms were developed from all combinations of interferometric pairs. The detectability of the boulder movements was assessed by comparing cumulative distributions of phase values from pixels covering the boulder after it was moved to: (1) the phase distribution of pixels in the surrounding non-moving portion of the image, and (2) the distribution of the boulder pixels phase values when the boulder was not moved.

4.2 Conclusions

      The results of this study showed that movements of boulders with nominal dimensions of 2 m and greater (up to about 5 m in this study) and located at offset distances in the range of 75 to 150 m could be detected using GBIR. Three boulders in this size range were monitored from two GBIR locations. Line of sight movements based on ground truth measurements ranged from as small as 1.7 mm to over 25 mm. For each of these three boulders, all of the movements were detected from both vantage points. The primary focus of this study was to evaluate the detectability of very small movements (e.g. 1-2 mm) that may be associated with precursor rockfall events. This magnitude of movement is of particular importance because other remote

sensing techniques that are able to cover large regions (such as photogrammetry and LiDAR) cannot detect movements that are this small. Based on the results from this study, GBIR appears to be a viable technique for this application. The findings from this study are only applicable to the offset range of about 75 to 150 m, as the spreading of the fan beam will decrease spatial resolution at larger range offset distances. Based on the results of this study, movements of boulders with dimensions of 2 m or greater were all detected in this study. However, detectability of smaller boulders (< 2m) was more challenging. The difficulty detecting smaller boulder was likely due to the presence of additional phase anomalies produced by the vegetation surrounding these smaller boulders. In these cases it was difficult to distinguish the anomalies caused by the boulder movements from those due to vegetation. Ongoing work is focusing on improving data collection and processing methods to remove or minimize phase contributions due to vegetation such that boulder movement detection thresholds can be improved.

References

Colorado Geological Survey (CGS), 2014. *Rockfall.* [Online] Available at:

http://coloradogeologicalsurvey.org/geologic-hazards/rockfall.

Colorado Geological Survey (CGS), 2008. Rockfall in Colorado. *RockTalk*. Colorado

Department of Natural Resources, 11(2).

Fielding, E.J., R.G. Blom, and R.M. Goldstein. 1998. "Rapid subsidence over oil fields measured

by SAR interferometry." *Geophysical Research Letters*, 25: 3215-3218

Gilliam, J. 2015. *"*Evaluation of Ground-Based Interferometric Radar for Detection of Small,

Localized Rockfall Movements in a Massive Landscape," M.S. Thesis, University of

Missouri (in progress).

Jenkins, W. 2013. *"*Evaluation of Ground-Based Interferometric Radar for Civil Engineering

Applications," M.S. Thesis, University of Missouri.

Jenkins, W., B.L. Rosenblad, F. Gomez, J. Legarsky and J.E. Loehr. 2012. "Deformation

Measurements of Earth Dams using Ground-Based Interferometric Radar (GBIR)."

Proceedings: Dam Safety 2012, Annual Meeting of the Association of State Dam Safety

Officials, Denver, CO

Ladd, G.E. 1935. "Landslides, Subsidence and Rockfalls." *Proceedings of the 36th Annual

Convention of the American Railway Engineering Association*, Chicago. 36; 1091-1163.

Lowry, B., F. Gomez, W. Zhou, M.A. Mooney, B. Held, and J. Grasmick. 2013. "High

resolution displacement monitoring of a slow velocity landslide using ground based radar

interferometry." *Engineering Geology*, 166: 160-169.

Massonnet, D., M. Rossi, C. Carmona, F. Adragna, G. Peltzer, K. Feigl, and T. Rabaute. 1993. "The displacement field of the Landers earthquake mapped by radar interferometry." *Nature*, 364:138 - 142.

Massonnet, D., P. Briole, and A. Arnaud. 1995. "Deflation of Mount Etna monitored by spaceborne radar interferometry." *Nature*, 375: 567-570.

Pritchard, M. E. and M. Simons, 2004. "Surveying volcanic arcs with satellite radar interferometry: The central Andes, Kamchatka, and beyond." *GSA Today,* 14: 4-10

Schmidt, D.A., and R. Bürgmann. 2003. "Time dependent land uplift and subsidence in the Santa Clara valley, California, from a large InSAR data set," *Journal of Geophysical Research*, 108. NO B9, 2416.

United States Geological Society (USGS), 2012. *Landslides in Colorado*, USA: Impacts and Loss Estimation for the Year 2010.